Controlling Size and Morphology in Hybrid Core@Shell and Core@Shell@Satellite Nanostructures for Sensing by Surface-Enhanced Raman Scattering

Journal:	*ACS Applied Nano Materials*
Manuscript ID	an-2020-016819.R1
Manuscript Type:	Article
Date Submitted by the Author:	n/a
Complete List of Authors:	Alarcón-Fernández, Carlos; University of Málaga, Department of Organic Chemistry Doña, Manuel; Universidad de Malaga, Organic Chemistry Tapia-Fernández, Antonio; Universidad de Malaga, Organic Chemistry Villaverde, Gonzalo; Complutense University of Madrid, Chemistry in Pharmaceutical Science Lopez-Ramirez, Maria Rosa; Universidad de Malaga, López-Romero, Juan Manuel; Universidad de Malaga, Contreras-Caceres, Rafael; Complutense University of Madrid, Chemistry in Pharmaceutical Science; Universidad de Malaga, Organic Chemistry

Controlling Size and Morphology in Hybrid Core@Shell and Core@Shell@Satellite Nanostructures for Sensing by Surface-Enhanced Raman Scattering

Carlos Alarcón-Fernández,[1] Manuel Doña,[1] Antonio Tapia-Fernandez,[1] Gonzalo Villaverde,[2] Maria Rosa Lopez-Ramirez,[3] Juan Manuel López-Romero,[1*] Rafael Contreras-Cáceres[1,2*]

[1] Department of Organic Chemistry, Faculty of Science, University of Málaga, 29071 Málaga, Spain.

[2] Department of Chemistry in Pharmaceutical Sciences, Faculty of Pharmacy, Complutense University of Madrid, Plaza Ramon y Cajal, 28040 Madrid, Spain

[3] Department of Physical Chemistry, Faculty of Science, University of Málaga, 29071 Málaga, Spain.

Abstract

Here we present the synthesis and characterization of a series of hybrid bimetallic core@shell and core@shell@satellites colloidal nanostructures. These nanosystems are structured as spherical and non-spherical metallic and bimetallic core encapsulated by a thermo-responsive N-Isopropylacrylamide (pNIPAM) shell (core@shell) with incorporated Ag satellites (core@shell@satellite). The metallic and bimetallic non-spherical cores include Au nanotriangles and bimetallic AuAg nanocubes, respectively. By using different amounts of $AgNO_3$ during chemical reduction and through the seed-mediated approach, we are able to modify the Ag satellites sizes. We include thermo-responsive surface enhanced Raman spectroscopy (SERS) investigations for core@shell and core@shell@satellite structures as a function of temperature, with improved SERS responses for the core@shell@satellite structure.

Keywords: Silver satellites, gold nanotriangles, bimetallic nanoparticles, hybrid structure, SERS enhancement.

INTRODUCTION

During the last years, the fabrication of hybrid stimuli-responsive nanosystems composed by a metal nanoparticle and a polymeric microgel has attracted considerable attention because these colloidal nanoparticles possess the sensing and catalytic advantages provided by the metal core and the highly colloidal stability and entrapment capabilities supplied by the polymer [1,2]. Compared with other types of colloidal structures used at the nanoscale level as dendrimers, silica and latex nanoparticles, polymer brushes or grapheme sheets, stimuli-responsive microgels offer the possibility to display sensitivity upon changes in some external parameter, as temperature [3], pH, [4] or even solvent nature and ionic strength [5]. It is well-known that the most synthesized stimuli-responsive microgel is poly(N-isopropylacrylamide) (pNIPAM), a thermoresponsive polymer that exhibits a phase transition from a hydrophilic water-swollen state to a hydrophobic globular state when is heated above its lower critical solution temperature (LCST), which is about 32ºC in water [6]. In general, concerning hybrid metal-polymer structures, one of the most reported hybrid system is organized as colloidal pNIPAM microgels in conextion with gold, silver or platinum nanoparticles [7–11]. Among different nanostructures, a very common reported structure is a colloidal system formed by pNIPAM acting as a core decorated with metal nanoparticles, which is described as a core@satellite structure [12–16]. The general approach for the synthesis of these core@satellite nanocomposites consists on the incorporation of metal ions into the pNIPAM microgel network, followed by a chemical reduction to Me^0 in presence of a strong reducing agent. For example, this core@satellite structure was fabricated by Ballauf who reported on polystyrene@pNIPAM cores with immobilized silver satellites (AgSTs) [17]. This core@satellite structure was also fabricated using methacrylic acid (MMA) as co-monomer during pNIPAM polymerization, thus supplying to the system pH responses [18]. More recently, Hellweg reported on the fabrication of core@satellite nanosystems by the incorporation of AgSTs into pNIPAM-derivative microgels [19]. Specifically, the core was fabricated with N-Isopropylacrylamide, N-isopropylmethacrylamide or N-n-propylacrylamide, and a polymeric shell containing poly-N-n-propylacrylamide. This core provided highly colloidal stability and controlled the diffusion of reactants towards the AgSTs.

Another important reported hybrid colloidal structure exhibits a core@shell structure. Essentially they are formed by a metal nanoparticle acting as a core homogeneously coated by a polymeric shell [20]. Using this structure, Carregal-Romero fabricated a

core@shell system formed by a 60 nm spherical gold nanoparticle encapsulated by pNIPAM (Au@pNIPAM) [21]. Later, based on the same core@shell morphology, Li fabricated a bimetallic AuAg core encapsulated by a pNIPAM shell by means a galvanic replacement [22]. It is important to mention that for the fabrication these core@shell–systems, a pioneer reported approach consisted on a metal surface functionalization with terminal vinyl groups [20]. Then, the core@shell structure is obtained by free radical polymerization of NIPAM in presence of a cross-linker molecule. By following this easy approach, 60 and 120 nm Au spheres were successfully coated by pNIPAM for sensing applications [21,23]. Later, by using an improved methodology, other morphologies as Au nanorod, nanoctahedra or nanotriangles were encapsulated by a pNIPAM shell [24,25]. Hybrid systems with a yolk-shell structure have been also fabricated. For example, thermo-responsive Au@pNIPAM yolk-shell systems in which a single Au nanoparticle is immobilized into a hollow pNIPAM shell have been also reported for catalytic application [26].

It is important to note that, apart from the previously described morphologies, during recent years, a new kind of colloidal nanostructured has appeared as the next generation of hybrid colloidal systems to be used as nanoreactors for catalysis and sensing investigations [27]. They are denoted as core@shell@satellite nanoparticles, and are structured as a metal core coated with a microgel shell, which is homogeneously decorated with small metal nanoparticles. Based on this structure, we have recently reported a methodology to obtain a core@shell@satellite colloidal system composed by a spherical bimetallic AuAg core, encapsulated by a pNIPAM shell containing AgSTs. This colloidal system was investigated for the catalytic reduction of 4-nitrophenol to 4-aminophenol at different temperatures [28], showing improved capabilities compared with core@shell structures. The methodology was based on a free radical polymerization using allylamine a co-monomer, thus enabling a subsequent coordination of Ag^{+} with the lone pair of electrons from NH_2, which were reduced to AgSTs by adding a strong reducing agent. However, this preliminary work included only one AgSTs size, as well as only spherical Au and bimetallic AuAg nanoparticles as nuclei. During the last years, pure Au and bimetallic AuAg nanoparticles have been synthesized including a great number of morphologies as spheres, rods, stars, octahedral, triangles or AuAg nanocubes. Recently, several protocols have been reported to encapsulate these metal nanoparticles with pNIPAM for different purposes, thus resulting in core@shell hybrid systems. However, the fabrication of core@shell@satellite structures containing

spherical or non-spherical morphologies has been barely reported. As is well-known, the fabrication of these hybrid system containing non-spherical and bimetallic cores is very promising. Concerning these new hybrid systems we have recently reported a protocol for the fabrication of core@shell@satellites strcutures with improved catalytic properties. However, we only included spherical morphogies as core. Importantly, the fabrication of core@shell@satellites strucutes containing non-spherical metal nanoparticles as core will improve their application because anisotropic structures have small angles and well-defined corners. In these areas the plasmon delocalization is more intense compares with spherical morphologies, thus leading improved Raman intensities compared with spherical morphologies [29,30]. Indeed, for SERS applications, silver nanoparticles are the most interesting nanoparticles due to they provide the strongest plasmon resonance. This effect is produced because the higher energy of the interband transition (~3,2 eV),[31] relative to the energy of the plasmon resonance, leads to minimum damping of the plasmon.

Here we include the first reported fabrication of core@shell@satellite structures containing gold nanotriangles as well as bimetallic AuAg nanocubes as core. The presence of the AgSTs improves the applicabilities in sensing as catalysis. Indeed, and additional improvement is the possibility to perform a temperature-controllable plasmon coupling between satellites as well as between core and satellise. This circumstance will remarkably improve sensing applicability due to the generation of hot spots. Initially we include the fabrication of core@shell and core@shell@satellite systems containing spherical as well as non-spherical cores, as Au nanotriangle (AuNTs) as well as bimetallic AuAg nanocubes (AuAgNCs). Indeed, we have varied the AgSTs sized by using different amount of $AgNO_3$ during chemical reduction, and by using the seed-mediated approach. Transmission electron microscopy images confirmed particle morphology, bimetallic composition as well as the AgSTs distribution within the microgels network. The presence of metal nanoparticles was also demonstrated by the plasmon band positions through UV-vis spectroscopy. Dynamic light scattering (DLS) investigations confirmed a different thermo-responsive behavior of core@shell systems compared with core@shell@satellite. The percentage of Au and Ag in each colloidal system was determined by thermogravimetric analysis (TGA). Finally, we have investigated the SERS responses for 4-mercaptobenzoic acid using core@shell and core@shell@satellites structures in function of temperature. Different response was found in every case, showing improved responses for the core@shell@satellite

structure. These fabricated core@shell@satellite particles offer important novelty aspects, as the presence of non-spherical metal nanoparticles as core, and the possibility to modify the AgSTs size, which could result a thermo-controllable core-satellite plasmon coupling, thus obtaining colloidal systems with improved plasmonic applications in several field as SERS, fabrication of optical sensors, and catalysis.

2. MATERIALS AND METHODS

2.1 Chemicals

Ascorbic acid (AA, 99%), cetyltrimethylammonium bromide (CTAB, ≥99%), benzyldimethylhexadecylammonium chloride (BDAC, 97%), 3-butenoic acid (3-BA, 97%), allylamine (98%), silver nitrate ($AgNO_3$, ≥99%), sodium borohydride ($NaBH_4$, ≥96%), and *N*-isopropylacrylamide (NIPAM, 97%) were supplied by Sigma-Aldrich. $HAuCl_4 \cdot 3H_2O$, trisodium citrate dihydrate, and sodium hydroxide (NaOH) were supplied as well by Sigma. *N,N′*-Methylenebisacrylamide (BIS, ≥99.5%) were supplied by Fluka. 2,2′-Azobis(2- methylpropionamidine)dihydrochloride (V50, 97%) was supplied by Acros Organics. All reactants were used without further purification. Water was purified using a Milli-Q system (Millipore).

2.2 Materials characterization

All UV−vis spectra were recorded using a Cary 50 scanning spectrophotometer (Varian, USA) with an incorporated xenon flash lamp by using a standard quartz cuvette (path length 1 cm). DLS was performed using a Malvern Zetasizer Nano S (Malvern Instruments, Malvern UK) using a detection angle of 173°. The intensity-averaged particle diameter and the polydispersity index values were calculated from cumulanttype analysis. Data were acquired after 5 min of sample dispersion and stabilization at each temperature (from 24 to 50 °C), with all measurements repeated three-fold. TEM investigations were performed by using a JEOL JEM 1400 (JEOL, Japan) operating at an acceleration voltage of 80 kV. Samples were prepared by drying 10 μL of each sample on a carbon-coated TEM grid. Tomography images were acquired on a JEOL JEM 2100 at an acceleration voltage of 200 kV. 3D-reconstruction of the tomography was carried out using the proprietary software. The Raman spectra were recorded in a Renishaw Invia micro-Raman spectrometer operating with a high power Renishaw NIR diode laser emitting at 785 nm. The microscope was equipped with a 50x objective (numerical aperture of 0.75). To avoid excessive heating during

measurement of Raman spectra and the possible thermal decomposition of the sample, neutral density filters with an optical throughput of 1% and 5% were used and the laser power at the sample was between 1 and 5 mW. The resolution was set at 4 cm^{-1} and the geometry of micro-Raman measurements was 180°. The Raman intensities have not been corrected for the spectral response of the instrument. The SERS samples of 4-Mercaptobenzoic acid (4MBA) at each temperature were measured in a 1 cm path length cell properly covered to avoid evaporation of the solvent reaching the final concentration of 10^{-4} M. A temperature sensor has been adapted to control the temperature of the bulk solution. The final volume was 500 μL in the mixture of colloids and adsorbate in water. The extended acquisition mode was used, from 100 to 3200 cm^{-1}. No accumulations were needed and the same experiment was repeted two times in order to validate the results that were very similar in each case. Samples were washed by centrifugation to remove the excess of 4MBA. Each experimente was repeated 3 times.

TGA analysis was performed by using a Mettler Toledo STAR system. After drying in the vacuum overnight, the composites were heated to 800 °C with a heating rate of 10 °C/min under N_2.

2.3 Synthesis of AuNSs@pNIPAM@Ag with controlled AgSTs sizes.

The encapsulation of gold nanospheres, AuNSs, within pNIPAM was performed in a two-step process. First, AuNSs with a mean diameter of ∼50 nm were prepared through a modification of the seeded-mediated growth method [32]. This method is based on the reduction of $HAuCl_4$ with 3-BA using ca. 15 nm CTAB-stabilized AuNS as seeds (, previously prepared by citrate reduction), in the presence of 0.015 M CTAB. Secondly, the pNIPAM polymer shell was grown by free radical polymerization in the presence of the previously synthesized vinyl-terminated AuNSs. To do that, Au colloidal dispersion (10 mL, 5 mM in terms of Au) was heated to 70°C under a N_2 flow. Then, the polymerization was carried out by introducing a monomer mixture composed by NIPAM (0.1698 g), the cross-linker BIS (23.2 mg, 10% in mols), and allylamine (7.5 μL, 8% in mol). After 15 min at 70 °C, the polymerization was started by adding 2,2′-azobis(2-methylpropionamidene)dihydrochloride (100 μL, 0.1 M). After 15 min, the reddish solution became turbid, the N_2 flow was removed and the reaction was allowed to proceed for 2 h at 70 °C. Then, the mixture was left to cool down at room temperature under magnetic stirring. In order to remove free microgels, as well as

oligomers and/or residual monomers produced during the polymerization process, the final colloidal sample was diluted with water (50 mL) and centrifuged (30 min at 4500 rpm). This step was repeated five times, and the final resulting pellet was redispersed in 10 mL of Milli-Q water, see scheme 1.

The fabrication of core@shell@satellite was performed by following a previously reported method [28]. However, in order to vary the AgSTs dimension we have performed the reduction in presence of different amount of $AgNO_3$. Briefly, in 10 mL of the previously prepared AuNSs@pNIPAM microgel dispersion, the appropriated amount of $AgNO_3$ was added at room temperature and medium magnetic stirring to reach 0.05, 0.3 and 0.875 mM $AgNO_3$ for samples denoted as AuNSs@pNIPAM@Ag_1, AuNSs@pNIPAM@Ag_2 and AuNSs@pNIPAM@Ag_3, respectively. Each solution was kept under these conditions during 30 min to allow a homogeneous coordination of Ag^+ ions with the amine groups from allylamine. Then, the reduction was achieved by adding 10, 60 and 175 μL of 50 mM $NaBH_4$ at room temperature and vigorous magnetic stirring to AuNSs@pNIPAM@Ag_1, AuNSs@pNIPAM@Ag_2 and AuNSs@pNIPAM@Ag_3, respectively. After 5 min, each solution was centrifuged at 5500 rpm during 30 min. The supernatant was discarded, and the pellet was redispersed in 10 mL of Milli-Q water. This cleaning process was repeated twice. Sample AuNS@pNIPAM@Ag_4 was performed by the seed mediated approach [33]. In detail, 5 mL of a solution composed by 0.4 M glycine buffer solution at pH 8.5 (adjusted by addition of NaOH, 1 M) and CTAB (200 mM) was mixed with 5 mL of the AuNSs@pNIPAM@Ag_3 system. Then, 100 μL of $AgNO_3$ (10 mM) were added under medium magnetic stirring. After 30 min, 50 μL of ascorbic acid (50 mM) as a mild reducing agent were added under vigorous magnetic stirring. The mixture was maintained under stirring for 30 min, followed by centrifugation (5500 rpm, 30 min). The supernatant was removed and the pellet was redispersed in 10 mL of MilliQ water, see scheme 1.

2.4 Synthesis of gold nanotriangles and gold nanooctahedra

The synthesis of gold nanotriangles, AuNTs, and gold nanooctahedra, AuNOs, was performed by following the same methodology previously reported by us [25]. Briefly, 100 mL of a mixture containing 1 mM $HAuCl_4$ and 5 mM BDAC was introduced into a 250 mL round bottom flask under low magnetic stirring (100 rpm). Then, the solution was heated up to 75 °C and then, 100 μL of 3-BA were added into the mixture. After

complete reduction of $HAuCl_4$ to Au^0 (followed by the absorbance at 400 nm) the solution was allowed to cool down to room temperature. Then, the excess of 3-BA and BDAC was removed by centrifugation at 7500 rpm for 30 min. The supernatant was discarded and the pellet was dispersed in 50 mL of 4 mM CTAC. This synthesis produces a mixture of nanooctahedra and nanotriangles (together with a small percentage of bigger particles, planar structures). Nanooctahedra and nanotriangles were purified by surfactant depletion-induced flocculation [34]. Specifically, the planar structures were firstly removed by centrifugation (7500 rpm for 30 min). Then, the resulting precipitate was redispersed in a 5 mL vial containing 2 mL of 100 mM CTAC. After 4 h at RT, a precipitate (containing bigger particles and planar morphologies) was observed at the bottom of the vial, which was discarded. The supernatant, containing a mixture of triangles and octahedra, was redispersed in 10 mL of 10 mM CTAC and again centrifuged at 7500 rpm for 30 min. Then, the supernatant was discarded and the pellet was redispersed in a 5mL vial containing 2 mL of 175mM CTAC. After 4h the supernatant, containing AuNOs, was separated, and the precipitate formed at the bottom of the vial, containing AuNTs, was redispersed in 10 mL of 100 mM CTAC. See scheme 2

2.5 Synthesis of core@shell@satellite AuNTs@pNIPAM@Ag microgels

Initially, the encapsulation of AuNTs within pNIPAM (core@shell AuNTs@pNIPAM) was performed by a small modification of a methodology previously reported by some of us [25,28]. Briefly, 10 mL of an AuNTs colloidal dispersion with [Au] ≈ 5 mM was heated at 70 °C under a N_2 flow. Then, *N*-isopropylacrylamide (0.1698 g, 100 mM), *N,N′*-methylenebisacrylamide (0.0234 g, 10 mM) and allylamine (7.5 μL, 8% in mol) were added under magnetic stirring (400 rpm). Then, the polymerization was initiated by adding 2,2′-azobis(2-methylpropionamidine) dihydrochloride (100 μL, 0.1 M in water), and after 15 min, the N_2 flow was removed and the polymerization was kept during 2 h at 70 °C. Then, the mixture was left to cool down at room temperature under magnetic stirring. In order to remove free microgels (pNIPAM without AuNTs core), as well as oligomers and/or residual monomers, the final colloidal sample was diluted with water (50 mL) and centrifuged 5 times 30 min at 4500 rpm. The final resulting pellet was redispersed in 10 mL of Milli-Q water. See scheme 2 (route 1)

For the incorporation of AgSTs into the microgel network 2 mL of the previously prepared AuNTs@pNIPAM microgels were diluted with 3 mL of water, then 25 μL of

29.4 mM $AgNO_3$ was added at RT and the mixture was magnetically stirring during 30 min. Then, 95 μL of 50 mM $NaBH_4$ was added under vigorous magnetic stirring. After 5 min, the solution was centrifuged at 5500 rpm during 30 min. Finally, the supernatant was discarded, and the pellet was redispersed in 5 mL of Milli-Q water. This cleaning process was repeated twice. See scheme 2 (route 1)

2.6 Synthesis of AuAg nanocubes

The synthesis of AuAg nanocubes, AuAgNCs, was carried out by following a small modification of a previously reported methodology [35]. In our case we used the previously purified AuNOs as seed for a Ag shell growth. Briefly, 50 mL of the AuNOs colloidal dispersion at 0.1 mM (in terms of Au) and 10 mM CTAC at medium magnetic stirring were introduced in a 100 mL round bottom flask that was immersed in an oil bath at 65ºC.. In order to avoid Ag nucleation, allowing a continuous growth on the Au surface, 4 mL of $AgNO_3$ (10 mM) and 4 mL of AA (40 mM) were added continuously in separate syringes at a rate of 0.166 mL/h. After 24h, the dispersion was left to cool down at room temperature, the AuAgNCs were centrifuged twice at 5500 rpm during 30 min, and redispersed in 50 mL of 15 mM CTAB. See scheme 2 (route 2)

2.7 Synthesis of AuAgNCs@pNIPAM@Ag microgels

The encapsulation of the AuAgNCs within a pNIPAM shell (core@shell AuAgNCs@pNIPAM) was achieved by following a similar approach previously reported elsewhere [25,28]. Briefly, 50 mL of the previously prepared colloidal dispersion containing AuAgNCs in 15 mM CTAB was heated at 70ºC. Then, 250 μL of 3-BA was added under medium magnetic stirring, and the mixture was maintained at these conditions during 1 h. After that, in order to remove the excess of 3-BA, the colloidal dispersion was centrifuged at 5500 rpm during 30 min. Then, the supernatant was discarded and the pellet was dispersed in 10 mL of 1 mM CTAB. This solution was again centrifuged at 5500 rpm during 30 min, the supernatant was discarded and the pellet was redispersed in 10 mL of Milli-Q water containing 250 μL of 5 mM CTAB. This dispersion was heated to 70 °C under a N_2 flow. Then, the polymerization was carried out by iadding the monomer mixture composed by NIPAM (0.1698 g, 100 mM), the cross-linker BIS (23.2 mg, 10 mM), and allylamine (7.5 μL, 8% in mol). Then, the polymerization was initiated by adding 2,2′-azobis(2-methylpropionamidene)dihydrochloride (100 μL, 0.1 M). After 15 min, the N_2 flow was

removed and the reaction was allowed to proceed during 2 h at 70 °C. After that, the mixture was left to cool down at room temperature under magnetic stirring. Then, free microgels, oligomers and/or residual monomers were removed by dilution with water (50 mL) and 5 x centrifugations (30 min at 4500 rpm). The final resulting pellet was redispersed in 10 mL of Milli-Q water. See scheme 2 (route 2)

For the incorporation of AgSTs into the microgel network (core@shell@satellites AuAgNCs@pNIPAM@Ag), 2 mL of the previously prepared AuAgNCs@pNIPAM particles were diluted with 3 mL of Milli-Q water, then 25 μL of 29.4 mM $AgNO_3$ was added at room temperature and medium magnetic stirring during 30 min. Then, 95 μL of 50 mM $NaBH_4$ was added at room temperature and vigorous magnetic stirring. After 5 min, the solution was centrifuged at 5500 rpm during 30 min. The supernatant was discarded, and the pellet was redispersed in 5 mL of Milli-Q water. This cleaning process was repeated twice. See scheme 2 (route 2)

3. Results and discussion

3.1 Spherical core@shell@satellites particles. Control on the AgSTs size

Scheme 1 shows schematic representation for the synthesis of core@shell@satellites systems containing spherical Au core. Initially, the synthesis of Au@pNIPAM microgels was performed by using 15 nm citrate-stabilized AuNSs as seeds to be grown to 50 nm spherical AuNSs, which are then treated with a molecule with a terminal double bond. Then, the presence of the monomers mixture composed by NIPAM, BIS and Allyl, generates a core@shell Au@pNIPAM system.

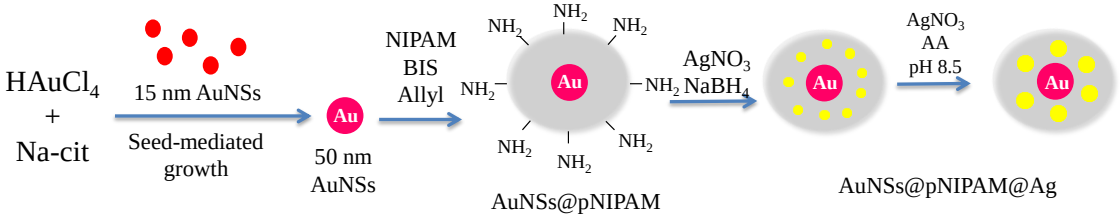

Scheme 1. Schematic representation for the synthesis of core@shell and core@shell@satellites containing AuNSs as nucleus.

Allylamine incorporates terminal NH_2 groups into the microgel network able to be coordinated with silver ions, and obtaining AgSTs into the microgel network after treatment with $NaBH_4$, thus resulting in a core@shell@satellite AuNSs@pNIPAM@Ag system. In order to vary the AgSTs size, we include in our investigation the AgSTs

fabrication by varying the amounts of $AgNO_3$. Figure 1A, 1B and 1C includes TEM images for samples denoted as AuNSs@pNIPAM@Ag_1, AuNSs@pNIPAM@Ag_2 and AuNSs@pNIPAM@Ag_3, respectively that correspond to core@shell@satellite fabricated under $AgNO_3$ 0.3, 0.5 and 0.875 mM. The measured particle size was 5.6 ± 2.4, 9.9 ± 3.9 and 13.6 ± 9.8 nm for AuNSs@pNIPAM@Ag_1, AuNSs@pNIPAM@Ag_2 and AuNSs@pNIPAM@Ag_3, respectively. We hypothesize that the increase in the AgSTs size is due to the higher amount of $AgNO_3$ used during satellites fabrication, as the ration of silver precursor ($AgNO_3$) and reducing agent ($NaBH_4$) was 1:1 in all cases. AgSTs size was measured by analyzing 100 AgSTs from TEM images. Figure S1 include particle distribution of AgSTs. Importantly, we were able to increase the AgSTs dimension by using the seed-mediated approach [33]. Basically, this method is based on the AgSTs overgrowth in presence of ascorbic acid into a buffer solution. By using this approach, we were able to increase the AgSTs size from 13.6 to 34.2 nm, as is shown in Figure 1D and S1D that correspond to the TEM image and the satellite size distribution for sample AuNSs@pNIPAM@Ag_4. A more detailed observation of TEM images shows that some microgels are not perfectly spherical. It is important to note that pNIPAM is a soft material, this microgel is not a hard sphere as polystyrene. During the drying process on the TEM grid the microgel does not totally collapses, and some residual water molecules are presented within the microgel network, thus resulting in a non-spherical morphology. This circumstance fits with previously reported works that demonstrate that the microgel sized obtained by dynamic light scattering (DLS) analysis at the collapsed state is lower compared with the microgel dimension measured by TEM [28,36] In Figure 1 some pNIPAM encapsulated microgels seem to be interconnected with thinner polymer bridges. This circumstance is produced because during the drying process of the sample drop on the TEM grid water evaporates, as microgels are subjected to Brownian motion some microgels can hit between them and some residual pNIPAM polymer can stick and form these polymeric wires.

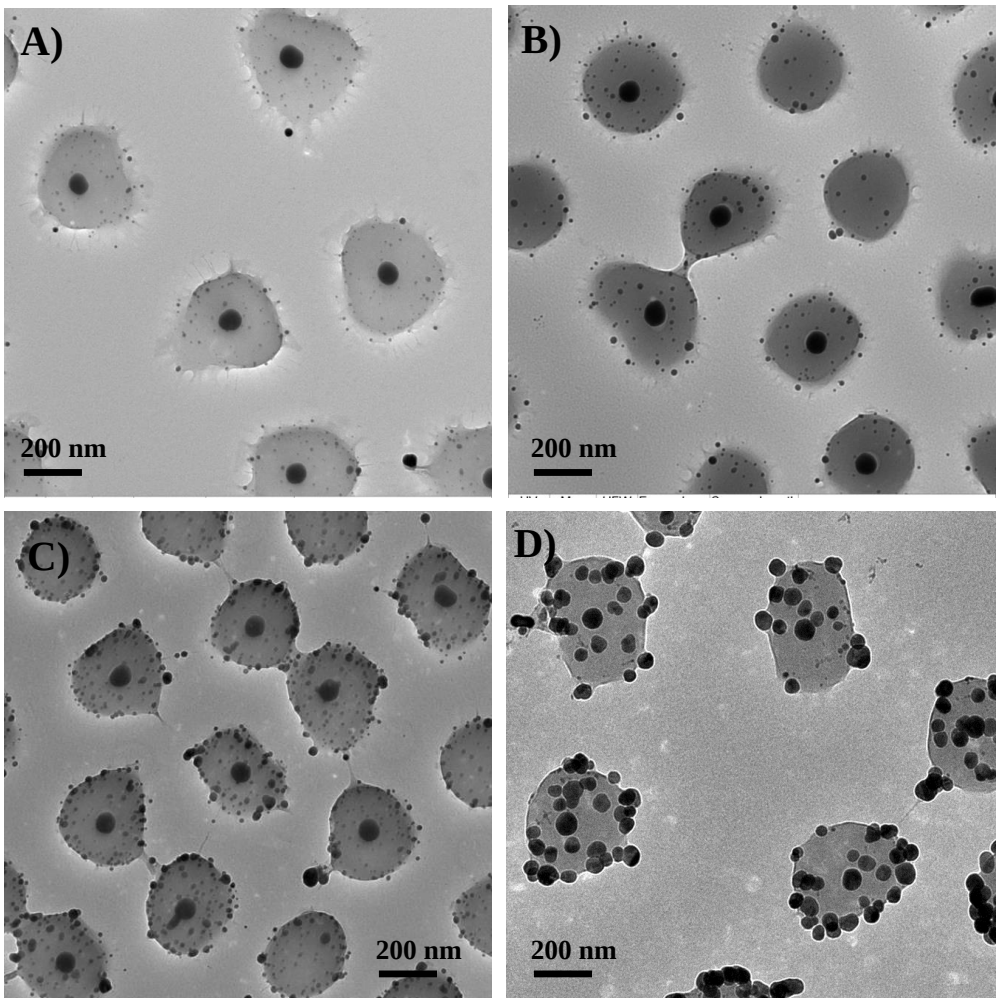

Figure 1. Representative TEM images of the core@shell@satellite microgels with spherical core: A) AuNSs@pNIPAM@Ag_1 and B) AuNSs@pNIPAM@Ag_2 and C) AuNSs@pNIPAM@Ag_3 and D) AuNSs@pNIPAM@Ag_4.

UV-vis spectroscopy has been also used to confirm the AgSTs growth. Figure S2 shows the normalized UV-vis spectra for the four obtained AuNSs@pNIPAM@Ag systems. All UV-vis spectra are normalized in the Au plasmon band in order to show the evolution of the Ag peak with the amount of $AgNO_3$. Initially, both Au (~535 nm) and Ag (~403 nm) plasmonic peaks can be observed for all specimens. However, the absorbance intensity of the Ag plasmon band increased with the AgSTs size. Specifically, the Ag/Au ratio of the plasmon band intensities increased with the amount of $AgNO_3$, 1.3, 1.5, 1.7 and 3.5 for AuNSs@pNIPAM@Ag_1, AuNSs@pNIPAM@Ag_2 and AuNSs@pNIPAM@Ag_3 and AuNSs@pNIPAM@Ag_4, respectively. As was reported and Mie´s theory establishes, the intensity of the plasmon band depends on the particle size[32]. It is important to note

that the width of the Ag plasmon band was related to the particle distribution. A metal colloidal dispersion with a wide particle distribution provides a wide plasmon band. Figure S1 includes the AgSTs size distribution after measuring 100 particles, which fits with the plasmon width. Figure S3 includes the UV-vis spectra for AuNSs@pNIPAM_3 and AuNSs@pNIPAM_4 samples at 25 and 50ºC. Interestingly, for the gold core, a plasmon displacement of 6 nm to longer wavelengths is observed in both cases. This shift is produced due to the different refractive index into the microgel network between both states (swollen and collapsed). However, the silver plasmon band shift induced by heating the colloidal samples was 5 and 9 nm for AuNSs@pNIPAM@Ag_3 and AuNSs@pNIPAM@Ag_4, respectively. The increase in the plasmon shift probably is due to the higher particle size (13.6 and 34.2, respectively).[24]

3.2 Non-spherical core@shell and core@shell@satellites particles.

The synthesis of non-spherical nanoparticles was achieved by using 3-BA as reducing agent and BDAC as surfactant that produces, at specific temperature, a mixture of AuNTs and AuNOs [25]. This particle combination is separated and purified by surfactant depletion induced flocculation [34]. In our work, concerning non-spherical nanoparticles, we have divided the synthesis of the different colloidal systems in route 1 and 2 (see Scheme 2). In route 1, after particle purification, the AuNTs were encapsulated with a pNIPAM shell obtaining a core@shell AuNTs@pNIPAM structure.. As mentioned, silver ions are able to coordinate with NH_2 groups from allylamine, and after the addition of $NaBH_4$, AgSTs are generated into the microgel network. However, for route 2, the separated AuNOs were firstly used as seeds for an Ag shell growth, thus resulting in bimetallic AuAg nanocubes (AuAgNCs). The bimetallic core was then encapsulated by a pNIPAM shell, thus obtaining a core@shell structure (AuAgNCs@pNIPAM) and, finally, AgSTs were incorporated into the microgel network obtaining a core@shell@satellite (AuAgNCs@pNIPAM@Ag) structure. Scheme 2 shows a schematic representation for the synthesis of the core@shell and core@shell@satellites containing non-spherical cores.

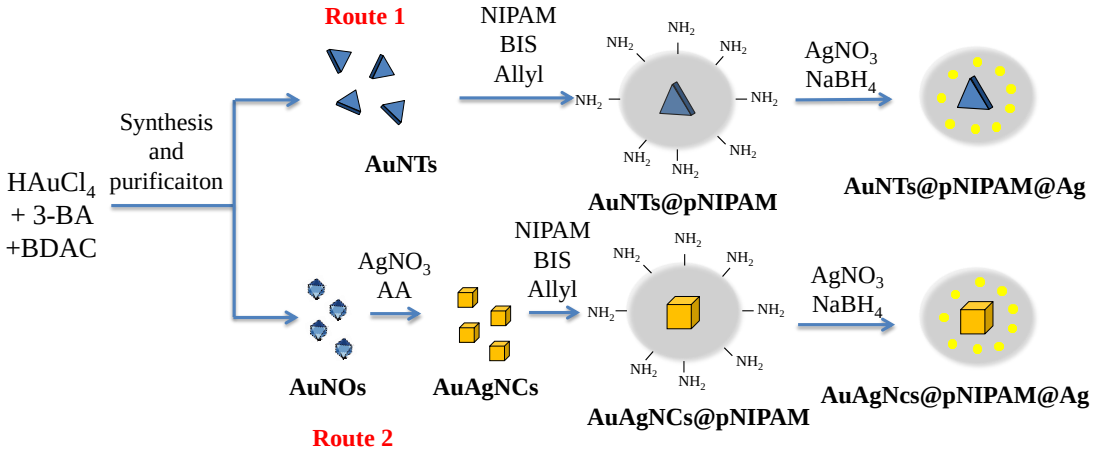

Scheme 2. Schematic representation for the synthesis of the different core@shell and core@shell@satellites colloidal systems containing a non-spherical core.

The successful fabrication of each non-spherical system was initially confirmed by TEM analysis. Figure 2 includes representative TEM images at two different magnifications of the initially fabricated and purified AuNTs and AuNOc. In both images, the percentage of triangles and octahedra is remarkably high, which confirms a highly effective particle separation. The measured particle dimension resulted in an average particles size of 55.5 ± 3.7 nm for AuNTs and 37.9 ± 2.3 nm for AuNOs.

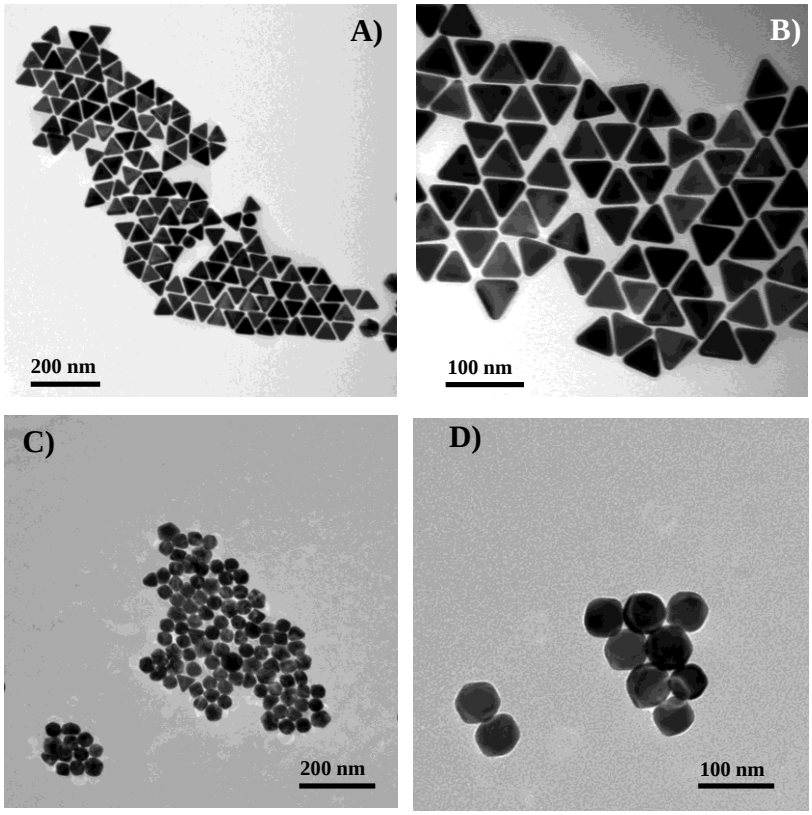

Figure 2. Representative TEM images non-spherical Au nanoparticles at different magnifications: A) and B) AuNTs and C) and D) AuOc.

Then, TEM images of the fabricated core@shell AuNTs@pNIPAM microgels (see scheme 2, route 1) are included in Figure 3A and 3B. Interestingly, a regular microgel shell surrounded an AuNTs was obtained, thus proving a homogenous pNIPAM polymerization. Interestingly Finally TEM images of the core@shell@satellite structure are included in Figure 3C and 3D. Well-distributed AgSTs in connection with the pNIPAM microgel can be appreciated, with an average particles size of 15.8 ± 3.9 nm, obtained after the analysis of 100 particles. Interestingly, the same interconnected polymer can be observed between some encapsulated pNIPAM microgels. We again believe that they are produced for the same reason than in Figure 1.

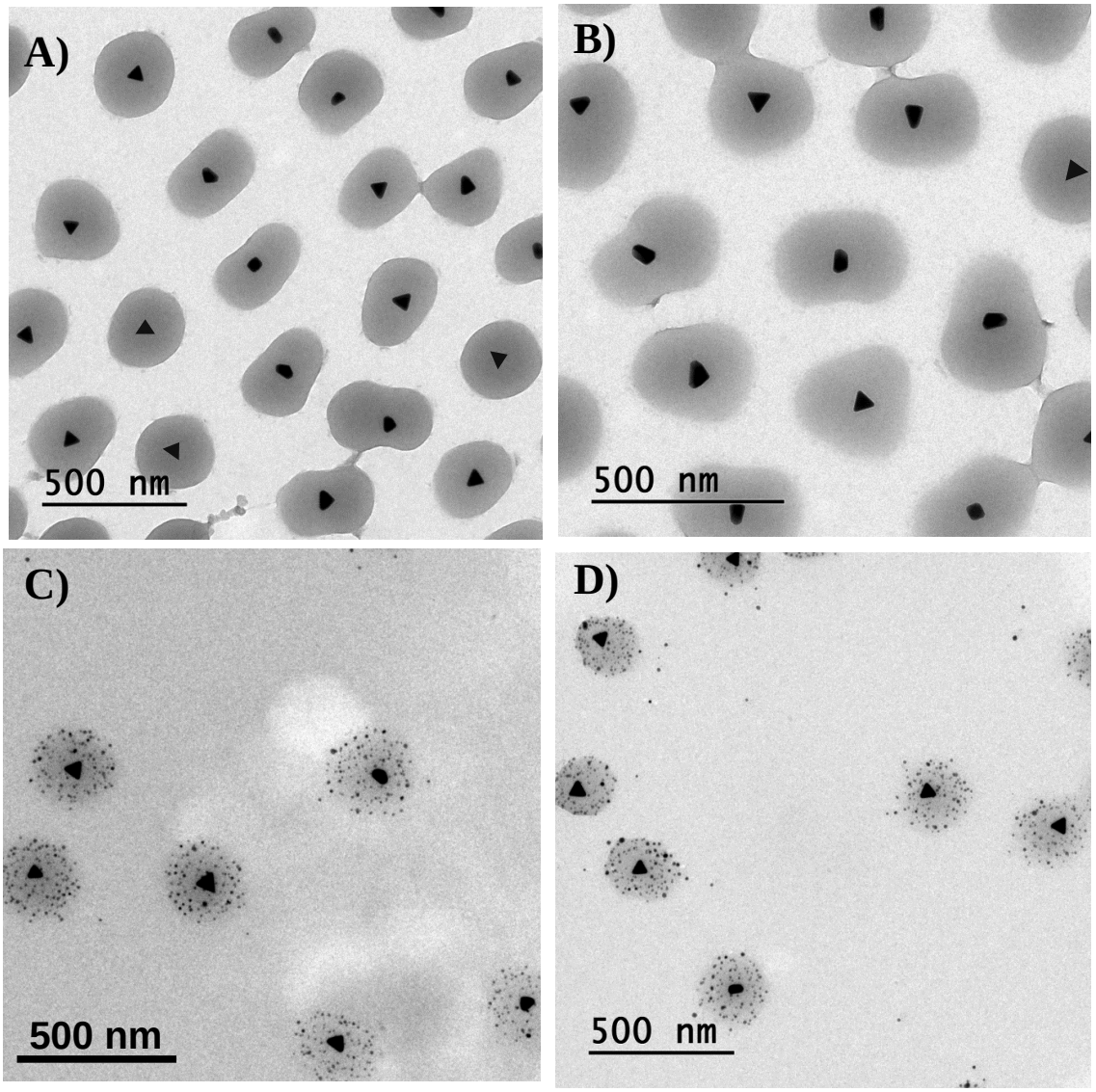

Figure 3. Representative TEM images at different magnification of the colloidal particles obtained in route 1. A) and B) core@shell AuNTs@pNIPAM and C) and D) core@shell@satellite AuNTs@pNIPAM@Ag microgels

The presence of Au and Ag was also confirmed by UV-vis spectroscopy. Figure S4 shows the normalized UV-vis spectra for the AuNTs (black line), the core@shell AuNTs@pNIPAM (red line) and the core@shell@satellite AuNTs@pNIPAM@Ag (blue line) particles. As expected, the isolated AuNTs exhibited a narrow in-plane (longitudinal) mode at 583 nm together with a broad out-of-plane (transversal) mode at 520 nm as a shoulder [37]. The normalized UV-vis spectrum for AuNTs after pNIPAM encapsulation (AuNTs@pNIPAM, red line) shows the two same bands of the non-coated AuNTs, which confirms the presence of the metallic core, and an increment in the absorbance intensity, due to the scattering produced for presence of the pNIPAM shell. Finally, the normalized UV-vis spectrum for the AuNTs@pNIPAM@Ag systems (blue line) exhibited both Au (~583 nm) and Ag (~403 nm) plasmonic peaks. Interestingly, the plasmon peaks at 583 and 520 nm are still observed.

The thermo-responsive capabilities of the core@shell and core@shell@satellite structures have been analyzed by DLS measurements. The shrinking ratio (the inverse of the swelling ratio) is defined as the ratio between the volume of the particle in the swollen state (at 24 °C) and the volume of the particle at each temperature [$\beta = V_{swollen}(24\ °C)/V(T)$] [20]. Figure S5 shows the shrinking ratio of the AuNTs@pNIPAM and AuNTs@pNIPAM@Ag systems as a function of temperature from 24 to 50ºC. As expected, for both systems, a well-defined volume transition is observed around 32 ºC. Interestingly, for the AuNTs@pNIPAM@Ag system a reduced swelling capability was obtained. This results fits with previously reported concerning spherical bimetallic AuAg@pNIPAM@Ag particles [28]. The explanation of this behavior is that the AgSTs incorporated into the pNIPAM network reduce the swelling−deswelling capability. In other words, the presence of the AgSTs hinders the microgel mobility during collapse, thus resulting in a lower swelling capacity. The amount of gold and silver was calculated by TGA analysis. Figure S6 represents the weight loss for AuNTs@pNIPAM@Ag microgel, the amount of Au and Ag obtained after heating the sample at 800 °C was 78%.

The colloidal structures obtained in route 2 were also initially identified by TEM analysis. Figure 4A and 4B includes TEM image for the bimetallic AuAgNCs system obtained after controlled Ag growth, using the previously synthesized AuOCs as seeds. As shown, monodispersed bimetallic nanocubes were obtained. The average AuAgNCs particle size (obtained after the analysis of 100 particles) resulted in 51.3 ± 3.2 nm Interestingly, Figure 4B shows the typical intensity contrast between the Au core and the Ag shell, produced by the electron scattering differences between both metals, and clearly reveals the presence of the octahedral Au core coated by a uniform Ag shell.. After pNIPAM polymerization, the successful microgel encapsulation is demonstrated in Figure 4C and 4D, which show the core@shell structure for AuAgNCs@pNIPAM particles showing the previously obtained AuAgNCs encapsulated by a polymer shell. Finally, the presence of the incorporated AgSTs in the core@shell@satellite structure is observed in Figure 4E and 4F. We have included in the SI a 3D tomography investigation for the AuAgNCs@pNIPAM@Ag systems that confirms a homogenous distribution of AgSTs into the microgel.

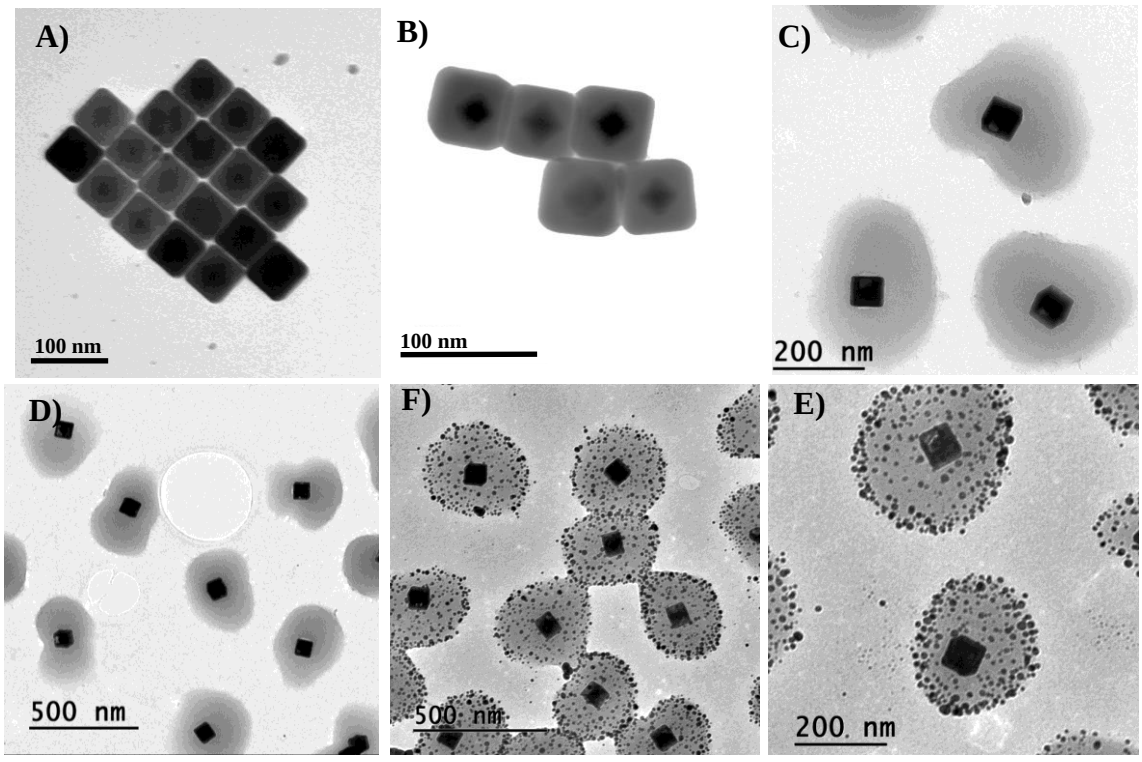

Figure 4. Representative TEM images of the different colloidal systems obtained in route 2. A) and B) AuAgNCs, C) and D) AuAgNCs@pNIPAM, E) and F) AuAgNCs@pNIPAM@Ag

Plasmon evolution was again confirmed by UV-vis analysis performed for the bimetallic structures fabricated in route 2. Figure 5A (black line) shows a well-defined plasmon peak centered at 543 nm corresponding to the normalized UV-vis spectrum for the initial AuNOs,. Then, after Ag growth (AuAgNCs, red line), the UV-vis spectrum dramatically changed by the presence of this metal into the colloidal structure. UV-vis showed a minimum at ca. 320 nm, characteristic of the interband transition in the Ag that damps the plasma oscillation in this spectral region [31,38,39]. The spectrum also revealed the presence of a plasmon resonance at ca. 420 nm, attributed to the formation of Ag. Indeed, the Au plasmon band drastically blue-shift to 495 nm due to the higher excitation cross-section of silver. The origin of such variation is assigned to the differences of Ag and Au, which results in a variation of the effective dielectric function of the bimetallic AuAg nanoparticle [40]. Additional higher-order plasmonic modes arising from the properties of pure AuAgNCs are found from 350 nm to 450 nm, which indicates low dispersity.[35] After microgel encapsulation (Figure 5B, black line) the core@shell AuAgNCs@pNIPAM systems only exhibited the plasmon peak at about 500 nm together with a weak shoulder about 400 nm, and the minimum corresponding to the interband transitions at ca. 320 nm. Finally, when AgSTs were included into the microgel (Figure 5B, red line) the normalized UV-vis spectrum showed a more intense plasmon band position (located at 410 nm) compared with the previous system, which confirms the presence of AgSTs into the colloidal structure.

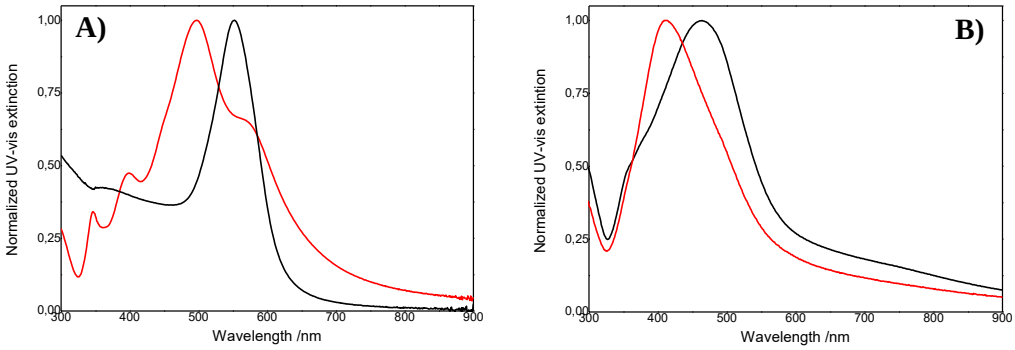

Figure 5. Normalized UV-vis extinction for: A) AuNOs (black line) and AuAgNCs (red line), B) AuAgNCs@pNIPAM (black line) and AuAgNCs@pNIPAM@Ag (red line).

3.3. SERS investigations

We have included a preliminary study concerning the SERS responses for core@shell (AuAgNCs@pNIPAM) and core@shell@satellite (AuAgNCs@pNIPAM@Ag) microgels. Figure S7 includes the Raman spectra of AuNCs@pNIPAM and AuNCs@pNIPAM@Ag systems. It can be observed the reference spectra of each colloid represented in the same range. We have initially chosen these systems for two principal reasons: *i)* as other metallic morphologies presented in literature, as triangles, stars or octahedral, the cube-like core also presents in this structure small angles and well-defined corners As is well-known, the plasmon deslocalization is more intense in structures with curvatures or high angles due to in these areas the increased in the local field or concentration of the electric field near the highly curved we hysurface[41], thus leading to improved Raman intensities compared with spherical morphologies, and *ii)* silver is the metal with the strongest plasmon resonance due to its higher energy of the interband transition (~3,2 eV) relative to the energy of the plasmon resonance, thus resulting to minimum damping of the plasmon. As mentioned, we have used 4-MBA as model analyte, and we have measured the SERS response at temperature from 25 to 75ºC. As a proof of concept, we also included a non-coated AuAgNCs colloidal system. Before SERS investigation, we measured the UV-vis spectra for AuAgNCs@pNIPAM and AuAgNCs@pNIPAM@Ag systems after the addition of 4-MBA. No differences were observed compared with the UV-vis spectra of pure colloidal dispersions. Figure S8 exhibits the SERS spectra for 4-MBA in the presence of the AuAgNCs systems in the mentioned range of temperatures showing two strong SERS bands at 1585 cm^{-1} (ring C–C stretching and C–H in-plane bending) and 1078 cm^{-1} (aromatic ring breathing, C–H in-plane bending and C–S stretching). Concerning the band at about 1410 cm^{-1}its origin it not clear because in this range both colloidal systems possess Raman signals, so it is difficult to distinguish Raman contribution from the adsorbate and from the colloidal systems. As can be seen it is a very weak band in both Figure 6A and 6B. As expected, this system provided a constant Raman intensity for both bands that remained unalterable at every temperature of analysis. On contrary, the SERS intensities for 4-MBA in the presence of core@shell AuAgNCs@pNIPAM and core@shell@satellite AuAgNCs@pNIPAM@Ag systems showed an interesting temperature-dependent behavior. Concerning the core@shell colloidal structure, the SERS intensity increased with the temperature of analysis from 25 to 42ºC, however, from this temperature, the SERS signal kept constant at any measured temperature (see

Figure 6A). In order to understand this behavior it is necessary to take into account that the SERS process depends on a long list of factors. It is traditionally accepted that two main enhancement mechanisms participate in the SERS phenomenon. The electromagnetic enhancement (EM), which relies on the large local field enhancements that occur close to metallic nanoparticles when localized surface plasmon resonances are excited[42]. EM enhancement does not require direct contact between the molecule and the metal, and decreases exponentially with distance from the surface. The dipole field decays with distance $1/d^3$, and is raised to the fourth power, thus giving results in dependence with $1/d^{12}$. Another contribution, believed to be much smaller than EM effect, is assigned to a chemical or charge-transfer effect (CT) that requires the molecules to be chemically adsorbed on the surface forming a metal-molecule complex[43]. As explained, pNIPAM experiments a phase transition at 32ºC in water. At 25ºC, below the LCST, pNIPAM remains in a total swollen state, and we consider that there are two different possibilities. At this state, 4-MBA molecules can be in contact with the silver surface or trapped within the polymer network, as is represented in Scheme 3 (left). By analyzing the SERS spectrum of 4-MBA we conclude that the carboxylate and the thiol groups of 4-MBA are deprotonated indicating that 4-MBA adsorbs on the Ag surface with a tilted orientation interacting through both functional groups[44]. As was previously reported, in neutral conditions of pH, 4-MBA usually adsorbs on metal nanoparticles surface as bideprotonated specie given rise to the typical SERS spectra we have shown in Figure 6 [44]. This adsorption behavior is similar in all the substrates here studied. When the temperature increases and the microgel collapses, the distance between the non-linked 4-MBA (represented in blue in Scheme 3) is reduced, thus increasing the SERS intensity as is predicted by the EM mechanism. When the microgel is totally collapsed (~42ºC) the distance molecule-surface particles cannot be reduced, thus resulting SERS intensity that not vary with temperature. As can be observed, a similar temperature-dependent behavior was obtained in the presence of the core@shell@satellite system. As for the previous core@shell system, the Raman intensity for 4-MA increases with the temperature of analysis (Figure 9B).” In both systems, after the SERS experiment, we measured the SERS signal after cooling the sample at room temperature. As expected, the same value that was the initially obtained before heating the sample was obtained, thus proving the reversibility of the fabricated systems[20]. As expected, due the AgSTs, the SERS intensity for 4-MBA is much higher compared with the previous core@shell system. At the beginning, the SERS intensity

increases with the temperature as in the previous case. However, the increment in the Raman intensity until 60ºC was probably due to the hindrance produced for the presence of AgNSs that are now more closer each other, and probably form aggregates in the collapsed state, thus resulting in an additional EM enhancement.

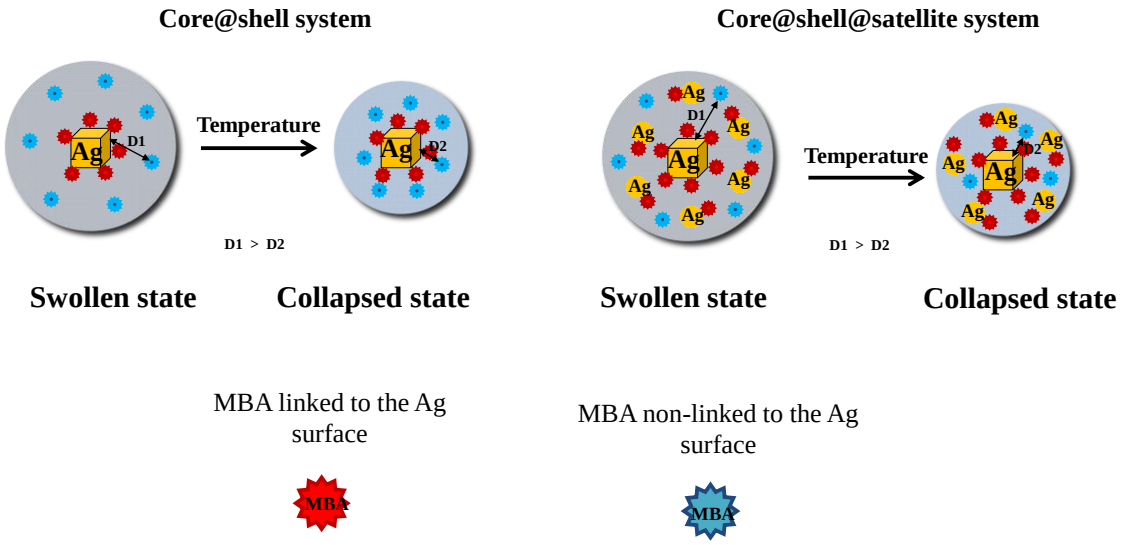

Scheme 3. Schematic representation for the two possible states of the 4-MBA molecules in presence of core@shell and core@shell@satellite colloidal systems

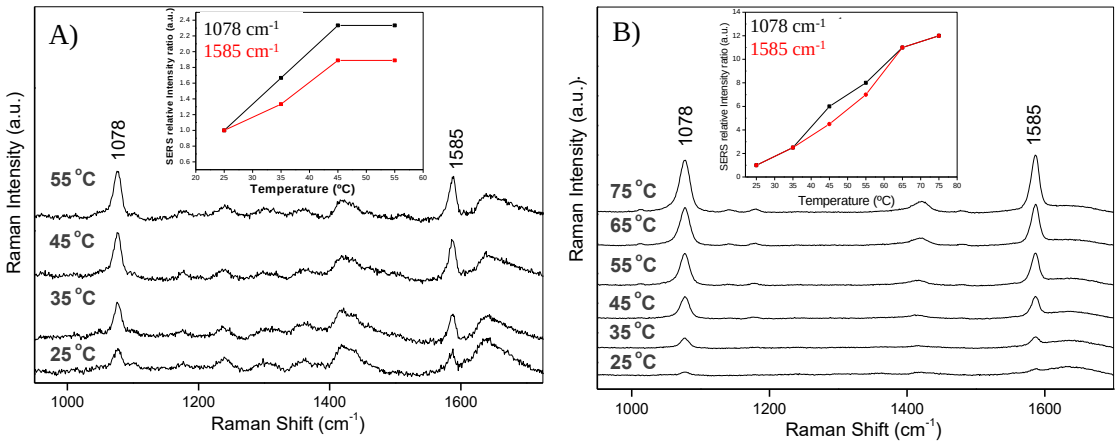

Figure 6. SERS spectra for 4-MBA at different temperatures in presence of A) core@shell and B) core@shell@satellite colloidal dispersion. The insets represent the relative intensities ratios for the bands at 1078 cm^{-1} (black line) and 1585 cm^{-1} (red line), which was normalized with respect to the Raman intensity at room temperature.

Finally, approximate enhancement factors (EF) of AuAgNCs@pNIPAM and AuAgNCs@pNIPAM@Ag colloidal dispersion were estimated by applying the equation $EF = (I_{SERS}\ V_{SERS}/\ I_{Raman}V_{Raman})\ f$,[45] where V_{SERS} and V_{Raman} represent the probed volumes, and I_{SERS} and I_{Raman} the intensities in SERS and Raman, respectively, "f" is the correction factor that considers the concentration ratio of the 4-MBA in both experiments under the same conditions. Figure S9 includes the calculated EF for Calculated EF for AuAgNCs@pNIPAM and AuAgNCs@pNIPAM@Ag colloidal structures.

4. Conclusion

Here we have presented the synthesis and characterization of a series of core@shell and core@shell@satellites thermo-responsive microgels. We fabricated colloidal structures containing spherical as well as non-spherical metallic and bimetallic cores. Specifically, for spherical cores (AuNS@pNIPAM@Ag), we were able to modify the AgSTs dimension by using different amounts of $AgNO_3$ during chemical reduction, and by the seed-mediated approach. Concerning non-spherical cores, two well-differentiated morphologies were encapsulated within a pNIPAM microgel shell, AuNTs and bimetallic AuAgNCs, both of them containing AgSTs. TEM and UV-vis spectroscopy were used to verify particle size, particle morphology as well as the distribution of AgSTs into the microgel. DLS measurements confirmed a different thermo-responsive capability between core@shell and core@shell@satellites structures. Importantly, the colloidal samples with incorporated AgSTs showed a shorter swelling transition due to the presence of the metal nanoparticles into the microgel network. Finally, we have proved that these structures have interesting SERS application as we are able to control the absolute SERS intensity of a target molecule by changing the temperature.

Supporting Information

Satellites distribution, UV-vis extinction of the core@shell@satellite sample with spherical core, for pure AuNTs, AuNTs@pNIPAM and AuNTs@pNIPAM@Ag microgels, shrinking ratio for the AuNTs@pNIPAM and the AuNTs@pNIPAM@Ag microgels, TGA analysis for AuNTs@pNIPAM@Ag microgels, Raman spectra for the AuNCs@pNIPAM and AuNCs@pNIPAM@Ag systems, SERS spectra for 4-MBA at different temperatures in presence of AuAgNCs particles and calculated EF for

AuAgNCs@pNIPAM and AuAgNCs@pNIPAM@Ag colloidal structures are included in the ESI.

5. Author information

Corresponding Authors

*E-mail: rcontreras@uma.es, rafcontr@ucm.es. Phone: +34951234236 (R.C.C.).

ORCID: 0000-0001-6313-2340

*E-mail: jmromero@uma.es. Phone: +34952137383 (M.L.R.).

ORCID: 0000-0003-2422-655X

Author Contributions

The manuscript was written through contributions of all authors. All authors have given approval for the final version of the manuscript. Authors declare no competing financial interest.

6. Acknowledgments

Authors acknowledge financial support from the Spanish MINECO project CTQ2016-76311. R.C.C. and G.V.C. acknowledge funding from the Comunidad de Madrid for the "Atraccion de Talento" project with reference 2018-T1/IND-10736.

References

(1) Roa, R.; Angioletti-Uberti, S.; Lu, Y.; Dzubiella, J.; Piazza, F.; Ballauff, M. Catalysis by Metallic Nanoparticles in Solution: Thermosensitive Microgels as Nanoreactors. *Zeitschrift fur Phys. Chemie* **2018**, *232* (5–6), 773–803. https://doi.org/10.1515/zpch-2017-1078.

(2) Lu, Y.; Mei, Y.; Schrinner, M.; Ballauff, M.; Möller, M. W.; Breu, J. In Situ Formation of Ag Nanoparticles in Spherical Polyacrylic Acid Brushes by UV Irradiation. *J. Phys. Chem. C* **2007**, *111* (21), 7676–7681. https://doi.org/10.1021/jp070973m.

(3) Schild, H. G. Poly(N-Isopropylacrylamide): Experiment, Theory and Application. *Prog. Polym. Sci.* **1992**, *17* (2), 163–249. https://doi.org/10.1016/0079-6700(92)90023-R.

(4) Sawai, T.; Yamazaki, S.; Ikariyama, Y.; Aizawa, M. PH-Responsive Swelling of the Ultrafine Microsphere. *Macromolecules* **1991**, *24* (8), 2117–2118.

https://doi.org/10.1021/ma00008a067.

(5) McPhee, W.; Tam, K. C.; Pelton, R. Poly(N-Isopropylacrylamide) Latices Prepared with Sodium Dodecyl Sulfate. *Journal of Colloid And Interface Science*. 1993, pp 24–30. https://doi.org/10.1006/jcis.1993.1075.

(6) Pelton, R. H.; Chibante, P. Preparation of Aqueous Latices with N-Isopropylacrylamide. *Colloids and Surfaces* **1986**, *20* (3), 247–256. https://doi.org/10.1016/0166-6622(86)80274-8.

(7) Lu, Y.; Mei, Y.; Drechsler, M.; Ballauff, M. Thermosensitive Core-Shell Particles as Carriers for Ag Nanoparticles: Modulating the Catalytic Activity by a Phase Transition in Networks. *Angew. Chemie - Int. Ed.* **2006**, *45* (5), 813–816. https://doi.org/10.1002/anie.200502731.

(8) Liu, G.; Wang, D.; Zhou, F.; Liu, W. Electrostatic Self-Assembly of Au Nanoparticles onto Thermosensitive Magnetic Core-Shell Microgels for Thermally Tunable and Magnetically Recyclable Catalysis. *Small* **2015**, *11* (23), 2807–2816. https://doi.org/10.1002/smll.201403305.

(9) Zhang, J.; Xu, S.; Kumacheva, E. Polymer Microgels: Reactors for Semiconductor, Metal, and Magnetic Nanoparticles. *J. Am. Chem. Soc.* **2004**, *126* (25), 7908–7914. https://doi.org/10.1021/ja031523k.

(10) Lu, Y.; Yuan, J.; Polzer, F.; Drechsler, M.; Preussner, J. In Situ Growth of Catalytic Active Au-Pt Bimetallic Nanorods in Thermoresponsive Core-Shell Microgels. *ACS Nano* **2010**, *4* (12), 7078–7086. https://doi.org/10.1021/nn102622d.

(11) Rehman, S.; Siddiq, M.; Al-Lohedan, H.; Sahiner, N. Cationic Microgels Embedding Metal Nanoparticles in the Reduction of Dyes and Nitro-Phenols. *Chem. Eng. J.* **2015**, *265*, 201–209. https://doi.org/10.1016/j.cej.2014.12.061.

(12) Zhang, C.; Li, C.; Chen, Y.; Zhang, Y. Synthesis and Catalysis of Ag Nanoparticles Trapped into Temperature-Sensitive and Conductive Polymers. *J. Mater. Sci.* **2014**, *49* (20), 6872–6882. https://doi.org/10.1007/s10853-014-8389-7.

(13) Satapathy, S. S.; Bhol, P.; Chakkarambath, A.; Mohanta, J.; Samantaray, K.; Bhat, S. K.; Panda, S. K.; Mohanty, P. S.; Si, S. Thermo-Responsive PNIPAM-Metal Hybrids: An Efficient Nanocatalyst for the Reduction of 4-Nitrophenol. *Appl. Surf. Sci.* **2017**, *420*, 753–763. https://doi.org/10.1016/j.apsusc.2017.05.172.

(14) Liu, Y. Y.; Liu, X. Y.; Yang, J. M.; Lin, D. L.; Chen, X.; Zha, L. S. Investigation of Ag Nanoparticles Loading Temperature Responsive Hybrid Microgels and Their Temperature Controlled Catalytic Activity. *Colloids Surfaces A Physicochem. Eng. Asp.* **2012**, *393*, 105–110. https://doi.org/10.1016/j.colsurfa.2011.11.007.

(15) Tang, Y.; Wu, T.; Hu, B.; Yang, Q.; Liu, L.; Yu, B.; Ding, Y.; Ye, S. Synthesis of Thermo- and PH-Responsive Ag Nanoparticle-Embedded Hybrid Microgels and Their Catalytic Activity in Methylene Blue Reduction. *Mater. Chem. Phys.* **2015**, *149*, 460–466. https://doi.org/10.1016/j.matchemphys.2014.10.045.

(16) Li, K.; Chen, X.; Wang, Z.; Xu, L.; Fu, W.; Zhao, L.; Chen, L. Temperature-Responsive Catalytic Performance of Ag Nanoparticles Endowed by Poly (*N* -Isopropylacrylamide- *Co* -Acrylic Acid) Microgels. *Polym. Compos.* **2017**, *38* (4), 708–718. https://doi.org/10.1002/pc.23630.

(17) Lu, Y.; Mei, Y.; Ballauff, M.; Drechsler, M. Thermosensitive Core-Shell Particles as Carrier Systems for Metallic Nanoparticles. *J. Phys. Chem. B* **2006**, *110* (9), 3930–3937. https://doi.org/10.1021/jp057149n.

(18) Farooqi, Z. H.; Begum, R.; Naseem, K.; Rubab, U.; Usman, M.; Khan, A.; Ijaz, A. Fabrication of Silver Nanoparticles in PH Responsive Polymer Microgel Dispersion for Catalytic Reduction of Nitrobenzene in Aqueous Medium. *Russ. J. Phys. Chem. A* **2016**, *90* (13), 2600–2608. https://doi.org/10.1134/S0036024416130239.

(19) Brändel, T.; Sabadasch, V.; Hannappel, Y.; Hellweg, T. Improved Smart Microgel Carriers for Catalytic Silver Nanoparticles. *ACS Omega* **2019**, *4* (3), 4636–4649. https://doi.org/10.1021/acsomega.8b03511.

(20) Contreras-Cáceres, R.; Sánchez-Iglesias, A.; Karg, M.; Pastoriza-Santos, I.; Pérez-Juste, J.; Pacifico, J.; Hellweg, T.; Fernández-Barbero, A.; Liz-Marzán, L. M. Encapsulation and Growth of Gold Nanoparticles in Thermoresponsive Microgels. *Adv. Mater.* **2008**, *20* (9), 1666–1670. https://doi.org/10.1002/adma.200800064.

(21) Carregal-Romero, S.; Buurma, N. J.; Pérez-Juste, J.; Liz-Marzán, L. M.; Hervés, P. Catalysis by Au@pNIPAM Nanocomposites: Effect of the Cross-Linking Density. *Chem. Mater.* **2010**, *22* (10), 3051–3059. https://doi.org/10.1021/cm903261b.

(22) Li, L.; Niu, R.; Zhang, Y. Ag–Au Bimetallic Nanocomposites Stabilized with

Organic–Inorganic Hybrid Microgels.Pdf. *RSC Adv.* **2018**, *8*, 12428–12438. https://doi.org/10.1039/c8ra01343h.

(23) Álvarez-Puebla, R. A.; Contreras-Cáceres, R.; Pastoriza-Santos, I.; Pérez-Juste, J.; Liz-Marzán, L. M. Au@pNIPAM Colloids as Molecular Traps for Surface-Enhanced, Spectroscopic, Ultra-Sensitive Analysis. *Angew. Chemie - Int. Ed.* **2009**, *48* (1), 138–143. https://doi.org/10.1002/anie.200804059.

(24) Contreras-Cáceres, R.; Pastoriza-Santos, I.; Alvarez-Puebla, R. A.; Pérez-Juste, J.; Fernández-Barbero, A.; Liz-Marzán, L. M. Growing Au/Ag Nanoparticles within Microgel Colloids for Improved Surface-Enhanced Raman Scattering Detection. *Chem. - A Eur. J.* **2010**, *16* (31), 9462–9467. https://doi.org/10.1002/chem.201001261.

(25) Casado-Rodriguez, M. A.; Sanchez-Molina, M.; Lucena-Serrano, A.; Lucena-Serrano, C.; Rodriguez-Gonzalez, B.; Algarra, M.; Diaz, A.; Valpuesta, M.; Lopez-Romero, J. M.; Perez-Juste, J.; Contreras-Caceres, R. Synthesis of Vinyl-Terminated Au Nanoprisms and Nanooctahedra Mediated by 3-Butenoic Acid: Direct Au@pNIPAM Fabrication with Improved SERS Capabilities. *Nanoscale* **2016**, *8* (8), 4557–4564. https://doi.org/10.1039/c5nr08054a.

(26) Wu, S.; Dzubiella, J.; Kaiser, J.; Drechsler, M.; Guo, X.; Ballauff, M.; Lu, Y. Thermosensitive Au-PNIPA Yolk-Shell Nanoparticles with Tunable Selectivity for Catalysis. *Angew. Chemie - Int. Ed.* **2012**, *51* (9), 2229–2233. https://doi.org/10.1002/anie.201106515.

(27) Li, S.; Lin, D.; Zhou, J.; Zha, L. Preparation of Silver Nanoparticles Loaded Photoresponsive Composite Microgels and Their Light-Controllable Catalytic Activity. *J. Phys. Chem. C* **2016**, *120* (9), 4902–4908. https://doi.org/10.1021/acs.jpcc.5b11724.

(28) Tzounis, L.; Doña, M.; Lopez-Romero, J. M.; Fery, A.; Contreras-Caceres, R. Temperature-Controlled Catalysis by Core–Shell–Satellite AuAg@pNIPAM@Ag Hybrid Microgels: A Highly Efficient Catalytic Thermoresponsive Nanoreactor. *ACS Appl. Mater. Interfaces* **2019**. https://doi.org/10.1021/acsami.9b10773.

(29) Pastoriza-Santos, I.; Liz-Marzán, L. M. Colloidal Silver Nanoplates. State of the Art and Future Challenges. *J. Mater. Chem.* **2008**, *18* (15), 1724–1737. https://doi.org/10.1039/b716538b.

(30) Xue, C.; Métraux, G. S.; Millstone, J. E.; Mirkin, C. A. Mechanistic Study of

Photomediated Triangular Silver Nanoprism Growth. *J. Am. Chem. Soc.* **2008**, *130* (26), 8337–8344. https://doi.org/10.1021/ja8005258.

(31) Kreibig, U.; Vollmer, M. *Optical Properties of Metal Clusters*; Springer Series in Materials Science; Springer Berlin Heidelberg: Berlin, Heidelberg, 1995; Vol. 25. https://doi.org/10.1007/978-3-662-09109-8.

(32) Rodríguez-Fernández, J.; Pérez-Juste, J.; García De Abajo, F. J.; Liz-Marzán, L. M. Seeded Growth of Submicron Au Colloids with Quadrupole Plasmon Resonance Modes. *Langmuir* **2006**, *22* (16), 7007–7010. https://doi.org/10.1021/la060990n.

(33) Tzounis, L.; Contreras-Caceres, R.; Schellkopf, L.; Jehnichen, D.; Fischer, D.; Cai, C.; Uhlmann, P.; Stamm, M. Controlled Growth of Ag Nanoparticles Decorated onto the Surface of SiO2 Spheres: A Nanohybrid System with Combined SERS and Catalytic Properties. *RSC Adv.* **2014**, *4* (34), 17846–17855. https://doi.org/10.1039/c4ra00121d.

(34) Jana, N. R. Nanorod Shape Separation Using Surfactant Assisted Self-Assembly. *Chem. Commun.* **2003**, *9* (15), 1950–1951.

(35) Mayer, M.; Steiner, A. M.; Röder, F.; Formanek, P.; König, T. A. F.; Fery, A. Aqueous Gold Overgrowth of Silver Nanoparticles: Merging the Plasmonic Properties of Silver with the Functionality of Gold. *Angew. Chemie - Int. Ed.* **2017**, *56* (50), 15866–15870. https://doi.org/10.1002/anie.201708398.

(36) Contreras-Cáceres, R.; Schellkopf, L.; Fernández-López, C.; Pastoriza-Santos, I.; Pérez-Juste, J.; Stamm, M. Effect of the Cross-Linking Density on the Thermoresponsive Behavior of Hollow PNIPAM Microgels. *Langmuir* **2015**, *31* (3), 1142–1149. https://doi.org/10.1021/la504176a.

(37) Shuford, K. L.; Ratner, M. A.; Schatz, G. C. Multipolar Excitation in Triangular Nanoprisms. *J. Chem. Phys.* **2005**, *123* (11). https://doi.org/10.1063/1.2046633.

(38) Kumbhar, A. S.; Kinnan, M. K.; Chumanov, G. Multipole Plasmon Resonances of Submicron Silver Particles. *J. Am. Chem. Soc.* **2005**, *127* (36), 12444–12445. https://doi.org/10.1021/ja053242d.

(39) Wang, H.; Tam, F.; Grady, N. K.; Halas, N. J. Cu Nanoshells: Effects of Interband Transitions on the Nanoparticle Plasmon Resonance. *J. Phys. Chem. B* **2005**, *109* (39), 18218–18222. https://doi.org/10.1021/jp053863t.

(40) Liu, M.; Guyot-sionnest, P. Synthesis and Optical Characterization of Au/Ag Core/Shell Nanorods. **2004**, 5882–5888. https://doi.org/10.1021/jp037644o.

(41) Gersten, J.; Nitzan, A. Electromagnetic Theory of Enhanced Raman Scattering by Molecules Adsorbed on Rough Surfaces. *J. Chem. Phys.* **1980**, *73* (7), 3023–3037. https://doi.org/10.1063/1.440560.

(42) Aroca, R. *Surface-Enhanced Vibrational Spectroscopy | Spectroscopy | Analytical Chemistry | Chemistry | Subjects | Wiley*; Aroca, R., Ed.; John Wiley & Sons, Ltd, 2006.

(43) Roman-Perez, J.; Centeno, S. P.; López-Ramírez, M. R.; Arenas, J. F.; Soto, J.; López-Tocón, I.; Otero, J. C. On the Dual Character of Charged Metal-Molecule Hybrids and the Opposite Behaviour of the Forward and Reverse CT Processes. *Phys. Chem. Chem. Phys.* **2014**, *16* (42), 22958–22961. https://doi.org/10.1039/c4cp03984j.

(44) Ho, C. H.; Lee, S. SERS and DFT Investigation of the Adsorption Behavior of 4-Mercaptobenzoic Acid on Silver Colloids. *Colloids Surfaces A Physicochem. Eng. Asp.* **2015**, *474*, 29–35. https://doi.org/10.1016/j.colsurfa.2015.03.004.

(45) Alvarez-Puebla, R. A.; Dos Santos, D. S.; Aroca, R. F. SERS Detection of Environmental Pollutants in Humic Acid-Gold Nanoparticle Composite Materials. *Analyst* **2007**, *132* (12), 1210–1214. https://doi.org/10.1039/b711361g.

TOC Graphic

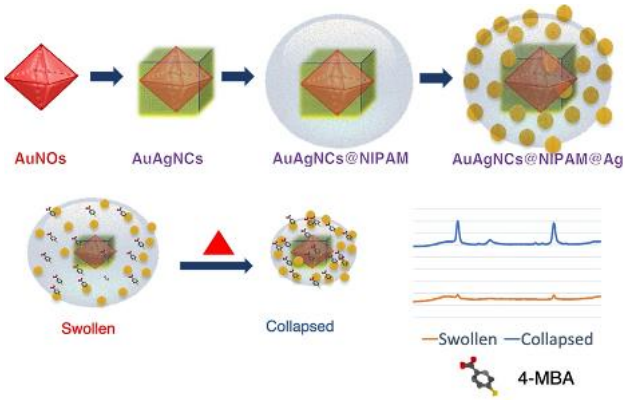
AuNOs
AuAgNCs
AuAgNCs@NIPAM
AuAgNCs@NIPAM@Ag
Swollen
Collapsed
Swollen
Collapsed
4-MBA

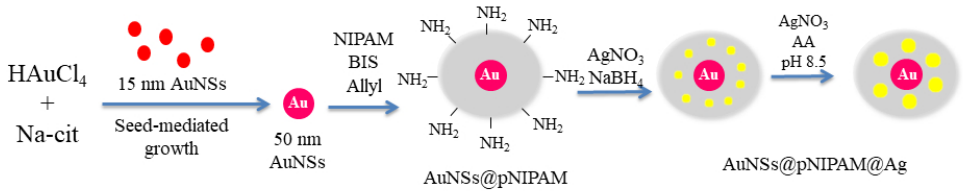

Scheme 1. Schematic representation for the synthesis of core@shell and core@shell@satellites containing AuNSs as nucleus.

254x190mm (96 x 96 DPI)

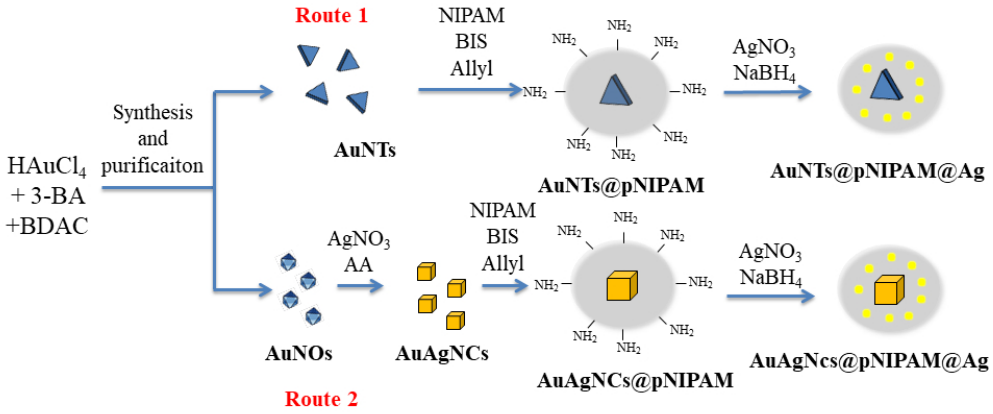

Scheme 2. Schematic representation for the synthesis of the different core@shell and core@shell@satellites colloidal systems containing a non-spherical core.

254x190mm (96 x 96 DPI)

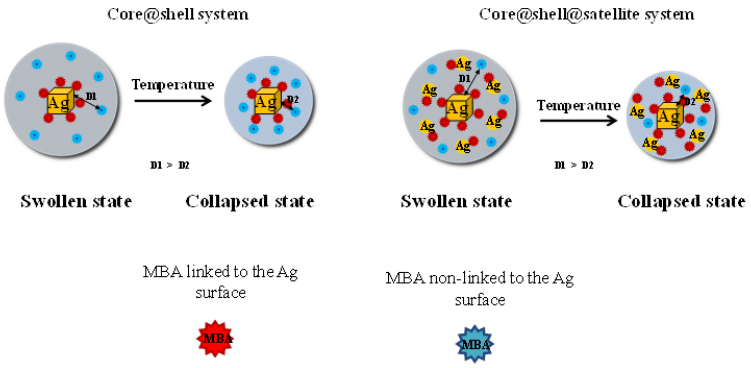

Scheme 3. Schematic representation for the two possible states of the 4-MBA molecules in presence of core@shell and core@shell@satellite colloidal systems

254x190mm (96 x 96 DPI)

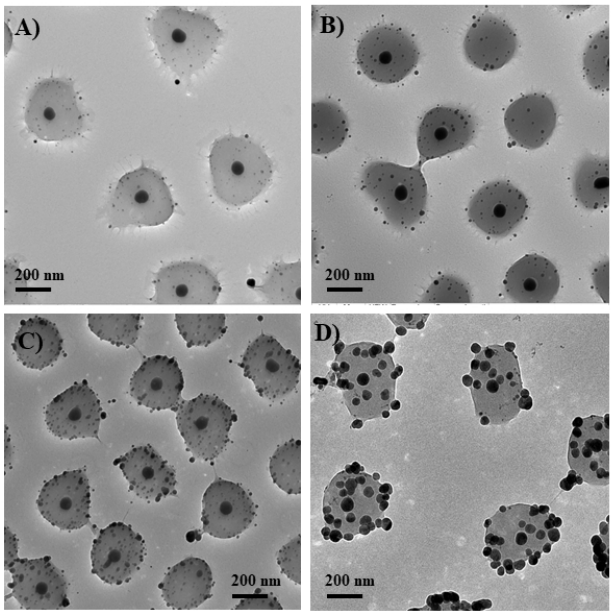

Figure 1. Representative TEM images of the core@shell@satellite microgels with spherical core: A) AuNSs@pNIPAM@Ag_1 and B) AuNSs@pNIPAM@Ag_2 and C) AuNSs@pNIPAM@Ag_3 and D) AuNSs@pNIPAM@Ag_4.

254x190mm (96 x 96 DPI)

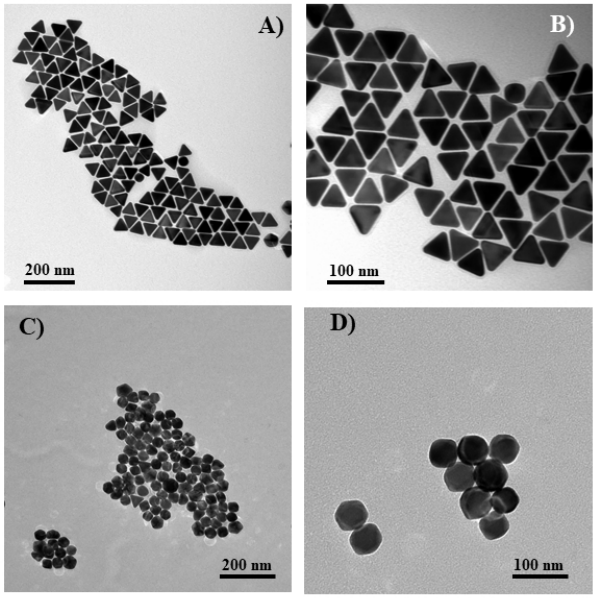

Figure 2. Representative TEM images non-spherical Au nanoparticles at different magnifications: A) and B) AuNTs and C) and D) AuOc.

254x190mm (96 x 96 DPI)

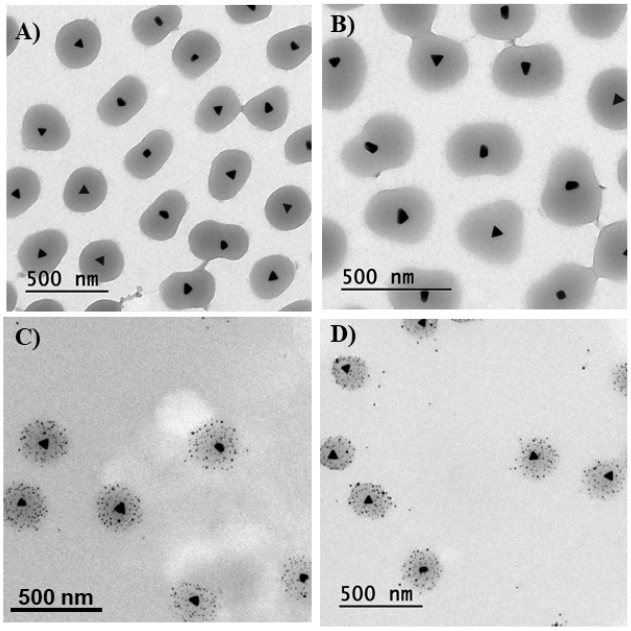

Figure 3. Representative TEM images at different magnification of the colloidal particles obtained in route 1. A) and B) core@shell AuNTs@pNIPAM and C) and D) core@shell@satellite AuNTs@pNIPAM@Ag microgels

254x190mm (96 x 96 DPI)

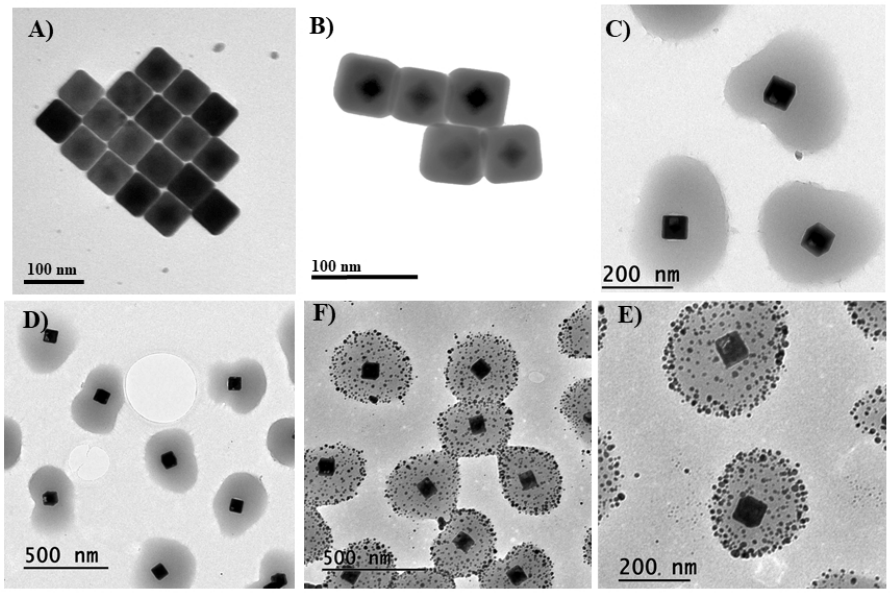

Figure 4. Representative TEM images of the different colloidal systems obtained in route 2. A) and B) AuAgNCs, C) and D) AuAgNCs@pNIPAM, E) and F) AuAgNCs@pNIPAM@Ag

254x190mm (96 x 96 DPI)

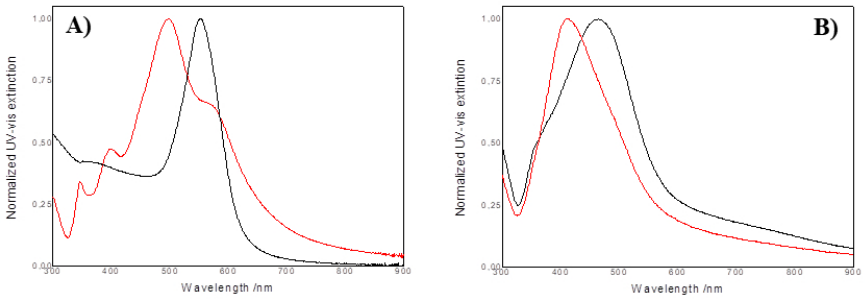

Figure 5. Normalized UV-vis extinction for: A) AuNOs (black line) and AuAgNCs (red line), B) AuAgNCs@pNIPAM (black line) and AuAgNCs@pNIPAM@Ag (red line).

254x190mm (96 x 96 DPI)

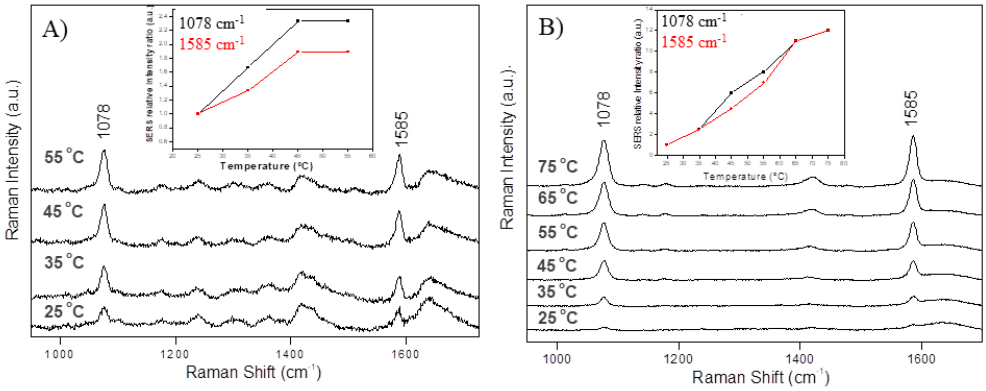

Figure 6. SERS spectra for 4-MBA at different temperatures in presence of A) core@shell and B) core@shell@satellite colloidal dispersion. The insets represent the relative intensities ratios for the bands at 1078 cm-1 (black line) and 1585 cm-1 (red line), which was normalized with respect to the Raman intensity at room temperature.

254x190mm (96 x 96 DPI)

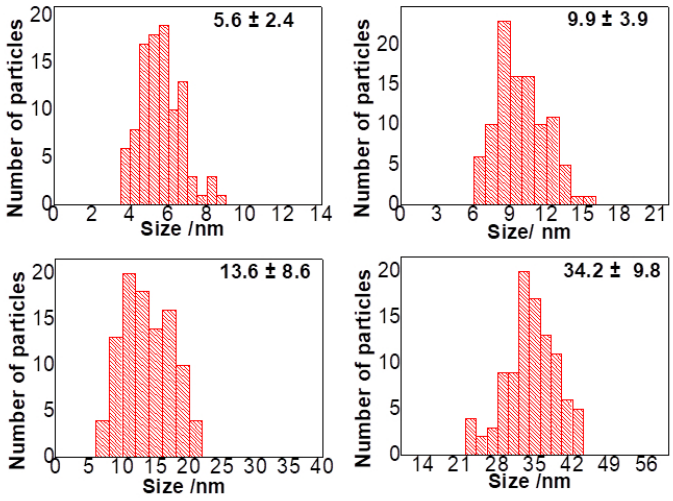

Figure S1. Particle distribution for of 100 NPs measured by TEM images of A) AuNSs@pNIPAM@Ag_1 and B) AuNSs@pNIPAM@Ag_2 and C) AuNSs@pNIPAM@Ag_3 and D) AuNSs@pNIPAM@Ag_4.

254x190mm (96 x 96 DPI)

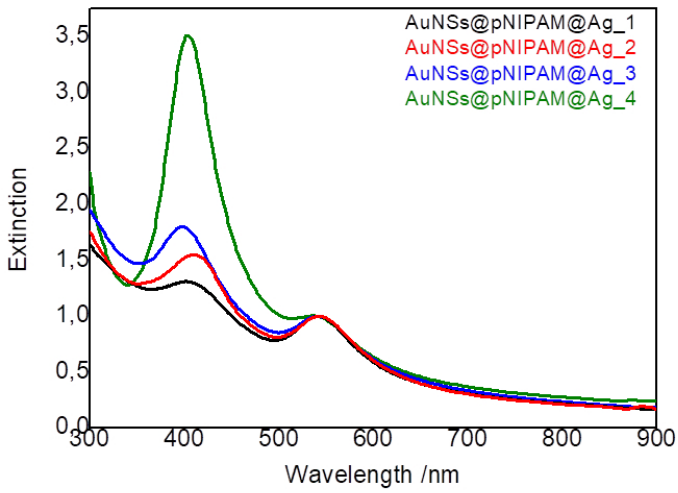

Figure S2. UV-vis extinction of the core@shell@satellite sample with spherical core. AuNSs@pNIPAM@Ag_1 (black line), AuNSs@pNIPAM@Ag_2 (red line), AuNSs@pNIPAM@Ag_3 (blue line) and AuNSs@pNIPAM@Ag_4 (green line)

254x190mm (96 x 96 DPI)

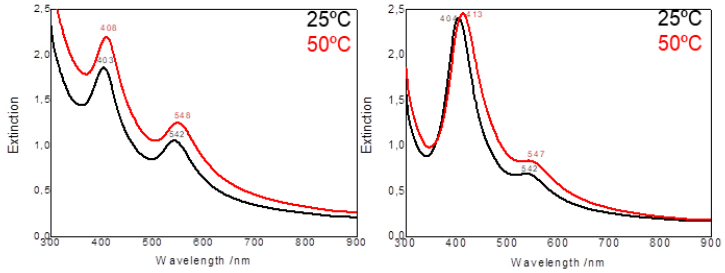

Figure S3. UV-Vis extinction spectra for AuNSs@pNIPAM@Ag aqueous hybrid colloids, below (25ºC, black lines) and above (50ºC, red line) the LCST A) AuNSs@pNIPAM@Ag_3 and B) AuNSs@pNIPAM@Ag_4

254x190mm (96 x 96 DPI)

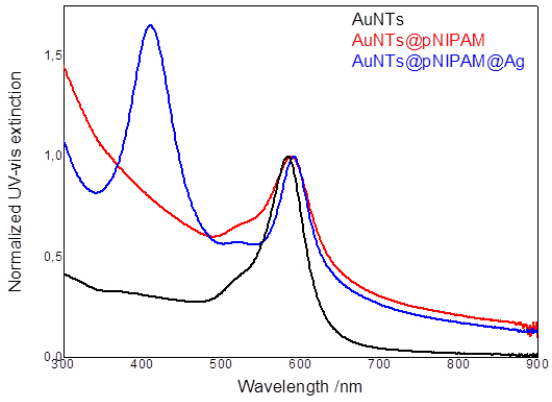

Figure S4. Normalized UV-vis extinction of the different systems obtained in route 1. Purified AuNTs (black line), AuNTs@pNIPAM (red line) and AuNTs@pNIPAM@Ag particles (blue line).

254x190mm (96 x 96 DPI)

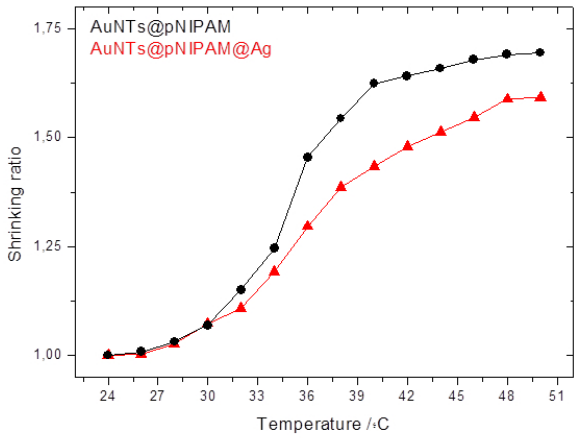

Figure S5. Shrinking ratio for the AuNTs@pNIPAM (black circles) and the AuNTs@pNIPAM@Ag (red triangles) microgels.

254x190mm (96 x 96 DPI)

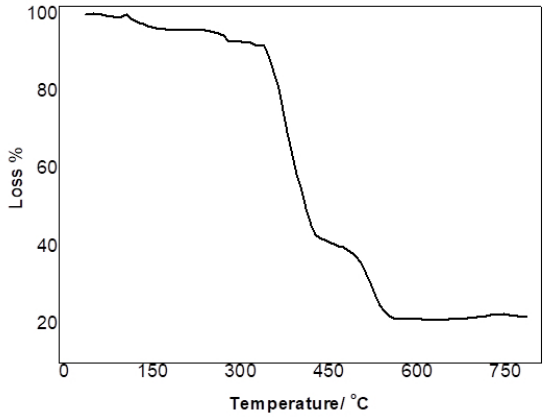

Figure S6. TGA analysis for AuNTs@pNIPAM@Ag microgels

254x190mm (96 x 96 DPI)

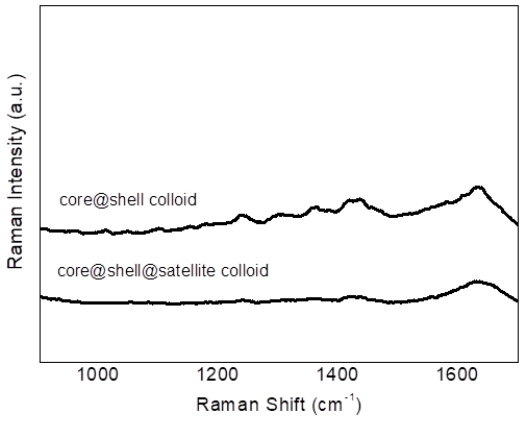

Figure S7. Raman spectra for the AuNCs@pNIPAM and AuNCs@pNIPAM@Ag systems.

254x190mm (96 x 96 DPI)

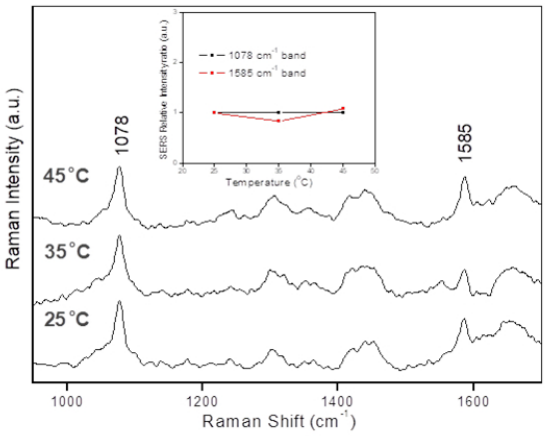

Figure S8. SERS spectra for 4-MBA at different temperatures in presence of AuAgNCs particles. The inset represents the intensities for the bands at 1078 and 1585 cm-1

254x190mm (96 x 96 DPI)

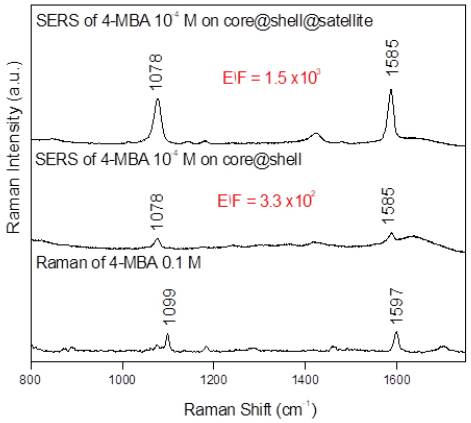

Figure S9. Calculated EF for AuAgNCs@pNIPAM and AuAgNCs@pNIPAM@Ag colloidal structures.

254x190mm (96 x 96 DPI)